Acceptance Averaging Effects on the Determination of the Response Functions

Brian Tighe [a,1]

[a] *Institut des Sciences Nucléaires*
IN2P3-CNRS/Université Joseph Fourier
38026 Grenoble cedex, France

Abstract

This report presents a comparative study of the statistical and the systematical errors on the determination of the response functions in parallel kinematics. On the base of the influence of the event rejection procedure, it is found that a certain set of windows in the virtual photon energy and momentum, and the missing momentum best compromise these uncertainties.

1 Introduction

In theory, the separation of coincidence cross sections into response functions is performed at some central kinematics; in experiment, of course, there is some acceptance range around that central kinematics. The experimental measure of the central kinematics is then an average over the acceptance range. Clearly the chosen acceptance range for averaging will influence specifically the statistical and systematic error in the measurement and generally the physical meaningfulness of any comparison between data and theory.

A Rosenbluth separation is particularly sensitive to such averaging effects, as it measures quantities which represent sums and differences of physical variables while considering equivalent acceptances in the forward and backward directions. Here, equivalent means that both directions accept identical ranges in those variables which describe the physics. As the forward kinematics tends

[1] Monroe Scolar of the College of William & Mary

to produce events over a wider range in these variables, the backward kinematics predominantly determines the acceptance range. To bring the acceptance ranges into accord, cuts in several variables are necessary.

This report shows the effectiveness of cuts in missing momentum, and virtual photon mass and energy for one selected parallel kinematics having $\mathrm{p_m} = 0$ MeV/c. Furthermore, the report develops a method to identify ranges for these cuts which compromise statistical and systematic errors in the response functions. The method generalizes to other parallel kinematics.

The choice of the physical parameters (or cuts) relevant to the $^3\mathrm{He(e,e'p)d}$ process at parallel kinematics is justified in the next section. Section 3 describes the influence of these cuts on several kinematical and physical variables using Monte Carlo simulations performed with MCEEP [1]. Section 4 characterizes the optimization of averaging effects with respect to statistical and systematic errors. Section 5 gives the conclusions.

2 Determinant Experimental Parameters

2.1 Cross Section & Response Functions

The five-fold differential cross section for the $^3\mathrm{He(e,e'p)d}$ process can be expressed as [2]

$$\frac{\mathrm{d}^5\sigma}{\mathrm{dE'd\Omega_e d\Omega_p}} = \frac{\mathrm{pE_p}}{(2\pi)^3}\,\frac{\sigma_\mathrm{M}}{\mathcal{R}}\;\mathcal{F}_\mathrm{structure} \tag{1}$$

where σ_M is the Mott cross section for a structureless $^3\mathrm{He}$ target nucleus

$$\sigma_\mathrm{M} = \left(\frac{\alpha}{2\mathrm{E}}\;\frac{1}{\sin\frac{\theta}{2}\tan\frac{\theta}{2}}\right)^2 \tag{2}$$

with $\alpha = 1/137$, the fine structure constant; $\mathcal{R}$ represents the so-called recoil factor which is written

$$\mathcal{R} = \left|1 - \frac{\mathrm{E_p}}{\mathrm{E_d}}\,\frac{\vec{\mathrm{p}}\cdot\vec{\mathrm{p}}_\mathrm{m}}{\mathrm{p}^2}\right|. \tag{3}$$

In the previous expressions, $(\vec{\mathrm{k}},\mathrm{E})$ is the 4-momentum of the electron beam, $(\vec{\mathrm{k}}',\mathrm{E}')$ is the 4-momentum of the scattered electron with scattering angle θ, and $(\vec{\mathrm{p}},\mathrm{E_p})$ is the 4-momentum of the struck proton having azimuthal angle ϕ with respect to the electron plane. The 4-momentum of the virtual photon is defined according to

$$\vec{q} = \vec{k} - \vec{k}' \tag{4}$$
$$\omega = E - E' \ . \tag{5}$$

$Q^2 = q^2 - \omega^2$ is the virtual photon mass, and its transverse linear polarization is written

$$\epsilon = \left[1 + \frac{2q^2}{Q^2}\tan^2\left(\frac{\theta}{2}\right)\right]^{-1} \ . \tag{6}$$

The deuteron 4-momentum is defined according to the usual momentum and energy conservation laws and is written

$$\vec{p}_m = \vec{q} - \vec{p} \tag{7}$$
$$E_d = \omega + M_{^3He} - E_p \ . \tag{8}$$

The structure function $\mathcal{F}_{\rm structure}$ accounts for the composite nature of the ^{3}He target nucleus and can be expressed as

$$\mathcal{F}_{\rm structure} = V_L R_L + V_T R_T + V_{TL} R_{TL} \cos(\phi) + V_{TT} R_{TT} \cos(2\phi) \tag{9}$$

with

$$V_L = Q^4/q^4 \tag{10}$$
$$V_T = Q^2/2\epsilon q^2 \tag{11}$$
$$V_{TL} = Q^3\sqrt{1+\epsilon}/q^3\sqrt{2\epsilon} \tag{12}$$
$$V_{TT} = Q^2/2q^2 \tag{13}$$

In parallel kinematics, the interference response functions vanish and the structure function reduces to

$$\mathcal{F}^{//}_{\rm structure} = V_L R_L + V_T R_T \ . \tag{14}$$

In the Plane Wave Impulse Approximation (PWIA), the reaction process can be understood as a direct interaction between the proton and the virtual photon while the recoiling deuteron plays a spectator role. Therefore, the response functions can be written as

$$R_i \propto \sigma_{ep} \ S(E_m, p_m) \tag{15}$$

where σ_{ep} is the cross section for the interaction of an electron with a free *moving* proton, and $S(E_m, p_m)$ is the spectral function describing the probability of finding a proton with momentum p_m and extraction energy E_m in the ^{3}He target nucleus. This factorization of the cross section makes it clear that the physics of the ^{3}He(e, e$'$p)d process depends on two *independent* sets of parameters: a first set describing the leptonic interaction, and a second one corresponding to the hadronic final sate.

It is desirable to make physically meaningful cuts on these sets, which preserve the largest possible number of events. The Rosenbluth separation requires *identical* forward and backward virtual photons, making ω, q and Q^2 all candidates for cuts, along with the Bjorken $x = Q^2/2m_p\omega$ variable (m_p is the proton mass), to define the leptonic part of the reaction. The Rosenbluth separation requires as well an *identical* hadronic part for the forward and backward measurements. On a more basic level, it is necessary to verify that events do in fact belong to the kinematics under study. This need prompts consideration of cuts in p, E_m, p_m, θ_{pq} (the angle between the struck proton and the virtual photon), and the out-of-plane angle ϕ.

2.2 Leptonic Parameters

Table 1 gives the kinematical parameters of the electron beam, of the scattered electron, and of the virtual photon for the chosen kinematics of this study. Fig. 1 shows histograms of the candidate variables, both in the forward and backward kinematics, for the description of the leptonic part of the interaction. These histograms provide a guide in determining the ranges in which cuts are to be made, and correspond to the phase space distribution of the events, that are unweighted by the physical cross section, for the ^{3}He(e, e′p)d process.

Table 1: leptonic kinematics parameters.

Kin.	E (GeV)	q (GeV/c)	ω (GeV)	θ (°)	E′ (GeV)	Q^2 (GeV^2)	x	ϵ
Σ_1	4.0450	1.000	0.4385	13.51	3.6065	0.8073	0.9811	0.9664
Σ_3	0.9950	1.000	0.4385	74.30	0.5565	0.8078	0.9817	0.4132

Two well specified parameters serve to fully describe the virtual photon, as its momentum and energy are not correlated. While an evident choice for these parameters is q and ω, Q^2 and x are possible as well. The matching of the forward and the backward phase space acceptances in ω (Fig. 1a) suggests a window (red lines) indicating a cut which selects relatively uniform distribution in both directions.

Identical requirements can be applied for the determination of the cuts in q (Fig. 1b). As expected, the comparison of the q distribution with and without (Fig. 1) the application of the previous ω cut does not show any change in the definition of the window in q, a direct consequence of the independence of q with respect to ω. This is definitely not the case for Q^2 which depends explicitely on ω: the same comparison (Fig. 1d and Fig. 1e) shows a small shift of the Q^2 window upon application of the ω cuts. Such an interdependence of cut parameters is cumbersome and undesirable. As x is also depending on ω, we eliminate both x and Q^2 from consideration and resolve to make leptonic cuts in q and ω.

2.3 Hadronic Parameters

Examination of Eq. (15) suggests that E_m and p_m are natural parameters to describe the physics of the hadronic part of the reaction. Since the present simulations deal only with the physical parameters *at the target* - the *true* event parameters - and concern specifically the 2-body breakup, the actual E_m distribution is a Dirac function at $E_m = 5.494$ MeV. When considering the *reconstructed* event parameters - the same physical parameters after the propagation in the spectrometer followed by the detection in the focal plane and the inverse propagation back to the interaction point - as well as other channels of the ^{3}He(e,e′p) reaction, a somewhat different and more explicit cut on E_m should be defined.

Table 2: hadronic kinematics parameters.

Kin.	p_m (GeV/c)	θ_p (°)	θ_{pq} (°)	p (GeV/c)
Σ_1	0.000	-57.43	0.00	1.000
Σ_3	0.000	-32.29	0.00	1.000

Table 2 gives the settings of the hadron spectrometer for the forward and backward measurements of the selected parallel kinematics. The corresponding phase space distribution in p_m can be seen in Fig. 2a. Since the Rosenbluth separation requires identical forward and backward acceptance, a basic cut in p_m (red line on the histogram) is readily obtained. However, it is not clear that this single cut is efficient enough to uniquely define the physics involved in the hadronic part of the interaction.

In the parallel kinematics, p describes a cone around q for some given θ_{pq}, with the circular base of the cone traced along the face of the spectrometer by a rotation in ϕ. Since the aperture of Hall A spectrometers is rectangular, events are rejected for some values of ϕ and accepted for others as θ_{pq} approaches the limits of the spectrometer's acceptance, resulting in a non-uniform acceptance in ϕ. An additional concern is the contamination of parallel kinematics events by non-parallel kinematics events allowed by the aperture of the spectrometers. The comparison between Eq. (9) and Eq. (14) shows that the resulting parallel structure function will be contaminated from interference response functions. In fact, that contamination appears to cancel if the previous cone around the virtual photon is uniformly detected. The most obvious means to eliminate the ϕ dependence is to introduce a cut in θ_{pq}; however, the correlation plot between ϕ and p_m on Fig. 2b suggests that a cut in p_m might serve equally well. As demonstrated on the histogram of the phase space distribution in ϕ on Fig. 2c, a p_m cut allows reduction of the observed peak effect, leading to a quasi-uniform distribution in ϕ. This feature is confirmed by the correlation spectra between θ_{pq} and p_m on Fig. 2d which shows explicitely that a cut in p_m is equivalent to the rejection of high θ_{pq} events, leading once again to a more uniform coverage of the cone.

The remaining parameter of the final hadronic state is the proton momentum. However, as shown in the correlation spectra between ω and p in Fig. 2e, a window in the proton momentum is equivalent to a window in the virtual photon energy. Therefore a further cut in p would not bring independent additional restriction on the event set.

3 Influence of Cut Parameters

Appropriately chosen cuts reduce the systematic error in the response functions, while the falling number of events, of course, increases statistic error. For increasingly stringent cut combinations, and given sufficient events, the mean values of the response functions should approach those of a single event having the same parameters as the kinematics under study (specified in Tables 1 and 2). As presented here, this manifests itself visually in an attraction towards the parameter's central value on the ordinate axis as one's eye moves from right to left and cyan to red in Fig. 3-8.

Those cuts applied here were chosen so as to be centered on the central kinematics, rather than to be symmetric with respect to the form of the spectra. These last cuts can select a more uniform phase space distribution; however, they shift the central point of the cut away from the central kinematics parameter. Such a shifting would be reflected in the average, which would tend towards not the central kinematics parameter but rather the central point of the cut window, especially as the window becomes increasingly narrow. This would make difficult any evaluation of the effectiveness of the cut. This evaluation for the chosen cuts is based on the examination of the variation of the mean value of a selected parameter $<$ Parameter $>$, as a function of then different cuts. This mean value is here defined according to

$$< \mathrm{Parameter} >= \sum_i \mathrm{n}_i \, \mathrm{P}_i \Big/ \sum_i \mathrm{n}_i \qquad (16)$$

where i is the bin index and n_i represents the number of events having the value P_i for the parameter under concern, after application of the chosen cuts.

Particularly,

$$N = \sum_i n_i \tag{17}$$

is the total number of events remaining in the parameter distribution after cuts. The statistical uncertainty attached to this mean value is written

$$\delta < \text{Parameter} >= \sqrt{\left(< \text{Parameter}^2 > - < \text{Parameter} >^2\right) / N} \tag{18}$$

where N directly reflects the number of events generated by MCEEP. For this report, MCEEP simulated 20,000,000 events in the forward direction and 1,000,000 in the backward, which yield comparable acceptances of about 1,000,000 at the spectrometer.

3.1 Averaged Kinematical Parameters

Fig. 3-4 show the mean value of the leptonic parameters of the reaction, excepting the selected cut parameters, as a function of the width of the ω window for a strict and a wide p_m cut.

In regarding the development of $< Q^2 >$, it is clear that there is little dependence on the ω cut for wide acceptances in p_m. Both forward and backward values progress slightly with deeper cuts in q, and seem to be approaching the central value; they are within 1 % after the first cuts. Some divergence is observed for small Δp_m and $\Delta\omega$, a trait shared with the spectra for x and ϵ. This is because the cut in ω does not act to reduce the acceptance in Q^2 (or x or ϵ); for these variables, the ω cut merely reduces the number of events without restricting more precisely the acceptance around the central value. The p_m and q cuts reduce the acceptance somewhat - and thus improve the average - but they compound the loss of events even further. As expressed by the large error bars, this apparent divergence should disappear for larger statistics.

$< x >$ shows light dependence on the ω cut in both directions. Values seem to converge towards the value of the central kinematics. $< x >$ develops the same divergence for strict cuts in p_m and ω as seen in $< Q^2 >$, specifically in the forward direction. It is sensible that the forward direction should display greater divergence than the backward, as the forward direction has a larger phase space acceptance (one of the reasons for applying cuts in the first place).

$< \epsilon >$ also converges to its central value under cuts, doing so quickly and with a light dependence on Δq. It also manifests divergence of the same origin as previously, under severe cuts. Note that, in contrast to $< Q^2 >$ and $< x >$, the forward and backward spectra converge to different values, as expected.

Fig. 5-6 shows the mean value of the hadronic parameters of the reaction as

a function of the p_m cut window around the central kinematics value (here 0) for a strict and a wide window in ω.
The $< \theta_{pq} >$ parameter exhibits a very nice behavior, quasi-unsensitive to Δq and $\Delta\omega$. As suggested by the physics, $< \theta_{pq} >$ shows a strong response to cuts in p_m and approaches its central value 0 in a regular fashion under increasingly strict cuts.
The development of $< p >$ presents an interesting picture. For small $\Delta\omega$ it shows a variation with Δp_m but not Δq, while for large $\Delta\omega$, which accepts a larger number of events, there exists variation in Δq and, more noticeably, larger statistical errors than the p_m window having less events. This seems to be due to the interplay between the statistics and the acceptance range when the number of events is globaly small. Indeed, cuts in p_m and q drastically reduce the number of events in the acceptance without altering the range of acceptance in p; conversely, cuts in ω reduce events more lightly while significantly narrowing the acceptance range in p. This narrowing in range more than compensates for the reduction in events, yielding smaller errors for stricter cuts in $\Delta\omega$. Note that this characteristic is not physically related to a specific window in ω; rather, it will be found varyingly depending on the total number of events in the spectrometer and should disappear for large statistics.

3.2 Averaged Response Functions

Fig.7-8 show the acceptance averaged value of each single contribution to the structure function. As required for a meaningful Rosenbluth separation, each contribution deconvoluted from its kinematical parameters should have the same value at forward and backward kinematics. In addition, for the separation in parallel kinematics to apply, the contributions of the interference response functions must be negligible.

The averaged longitudinal $< V_L R_L >$ and transverse $< V_T R_T >$ contributions show no sensitivity to cuts in ω or q and a consistent progression under cuts in p_m. This is the expression of the dependence of the response functions R_L and R_T in terms of p_m by means of the spectral function. However, $< V_L R_L >$ converges to the same value at forward and backward kinematics. $< V_T R_T >$ behaves somewhat differently since it does not converge to the same value in both directions. This results from the ϵ dependence of kinematical factor V_T. $< V_{TL} R_{TL} >$ and $< V_{TT} R_{TT} >$ show similar dependence in $\Delta\omega$ and Δp_m while a more pronounced sensitivity to Δq is observed. Once the ϵ dependence on V_{TL} is taken into account, the forward/backward consistency of $< V_{TL} R_{TL} >$ is obtained. In contrast, $< V_{TT} R_{TT} >$ do not converge to the same value in both directions. This is particularly true for large $\Delta\omega$ and Δp_m and results only from the rapid variation of R_{TT} in these parameters. As cited before, the consistency of the parallel Rosenbluth separation depends strongly on the minimization of the contamination from non-parallel kinematics events. For the present kinemtaics, it is found that any Δp_m cut below 60 MeV/c will result in a contamination level of the cross section from the sum $< V_{TL}R_{TL} >$ $+ < V_{TT}R_{TT} >$ of 1 % at most.

4 Statistical versus Systematical Efffects

Fig. 9-10 show the acceptance rates at forward (α = F) and backward (α = B) kinematics, defined as the ratio

$$A_\alpha = \frac{N}{N_0} = \frac{\text{Events within cuts}}{\text{Events in the spectrometers}} , \tag{19}$$

and the response function ratios for the longitudinal (β = L) and the transverse (β = T) contributions, defined as

$$B_\beta = \frac{2\ [< R_\beta >_{\text{backward}} - < R_\beta >_{\text{forward}}]}{< R_\beta >_{\text{backward}} + < R_\beta >_{\text{forward}}} \tag{20}$$

The acceptance rates indicate the event rejection resulting from cuts in each of the three determinant parameters. It is therefore partly connected to the statistical error on the cross section measurement; the full statistical error would involve in addition, the physics cross section, the electron beam flux and the data taking time. It is clear that the forward direction has a wider phase space distribution in the cut parameters, as its acceptance rates are generally a tenth of those in the backward direction. In addition, A_α are naturally strongly sensitive to these cuts.
The response function ratios express the consistency between the forward and backward measurement of the cross section and suggests a flavor of the systematical effects. Any non-zero ratio means that the theoretical average value of the response functions differs from forward to backward directions but does not tell how this variation affects the determination of the response functions from the averaged cross section. That last effect is understood as a true systematical error. B_β is, as exepected, quasi-unsensitive to the leptonic cuts and strongly dependent on Δp_m. It is guessed that the average effects on B_β should be kept below the 5 % level to insure a 2 % overall systematic uncertainty. This resctriction corresponds to a maximum Δp_m = 60 MeV/c, at the present kinematics, and would allow keeping 65 % of the maximum available phase space.

5 Conclusions

A method based on acceptance calculations using MCEEP has been developed with the aim to compromise statistical and systematic errors in parallel kinematics response functions. Three determinant kinematical paramaters have been identified for the selection of the physics process: ω, q, and p_m. The leptonic cuts cause little change in the average values of the response functions; the hadronic parameter p_m has here the greatest influence. This being the case, only light cuts in q and ω - such as the $\Delta q = 64$ MeV/c and $\Delta\omega = 47$ MeV windows demonstrated here - should be applied. A window in p_m of about 60 MeV/c guarantees parallel kinematics, having cross terms at least two orders of magnitude smaller than the longitudinal and transverse terms; moreover, about 65 % of the events are preserved, with respect to the lightest combination of cuts considered herein.

References

[1] P. Ulmer, *Monte Carlo for Electro-Nuclear Coincidence Experiments* **v2.3** (1999).

[2] J.J. Kelly, *Adva. in Nucl. Phys.* **23** (1996) 75.

Figure Captions

Figure 1: comparison of the forward (dashed line) and backward (full line) acceptances in ω (a), q (b), and Q^2 (c); the vertical red lines indicate the widest window in these parameters for the definition of the Rosenbluth phase space ($\Delta\omega$ = 47 MeV and Δq = 64 MeV/c) ; figures (c) and (e) give the phase space distribution of the events after application of the ω window: the red dashed line in (e) indicates the change in the definition of the Q^2 window upon this ω rejection.

Figure 2: comparison of the forward (dashed line) and backward (full line) missing momentum distribution (a); correlation between the out-of-plane angle and the missing momentum (b), the green and blue lines indicating the p_m cut values that lead to the coloured histograms of the ϕ distribution (e); correlation between the angle of the proton with respect to the virtual photon and the missing momentum (d), the red line indicating the p_m cut defined in (a); correlation between the virtual photon energy and the proton momentum (e), the red lines indicating the ω window defined in Fig. 1a.

Figure 3: averaged Q^2, x, and ϵ as a function of the ω window for the forward and backward kinematics at a fixed Δp_m = 90 MeV/c; the different curves correspond to different Δq windows.

Figure 4: same as Fig. 3 for Δp_m = 10 MeV/c.

Figure 5: averaged θ_{pq} and p as a function of the p_m window for the forward and backward kinematics at a fixed $\Delta\omega$ = 3 MeV; the different curves have the same meaning as in Fig. 3.

Figure 6: same as Fig. 5 for $\Delta\omega$ = 47 MeV.

Figure 7: averaged single contributions of the response functions to the cross section as a function of the p_m window for the forward and backward kinematics at a fixed $\Delta\omega$ = 3 MeV; the different curves have the same meaning as in Fig. 3.

Figure 8: same as Fig. 7 for $\Delta\omega$ = 47 MeV.

Figure 9: statistical and systematical ratios, as defined in the text, as a function of the p_m window for the forward and backward kinematics, and the longitudinal and the transverse response functions, at a fixed $\Delta\omega$ = 3 MeV; the different curves have the same meaning as in Fig. 3.

Figure 10: same as Fig. 9 for $\Delta\omega$ = 47 MeV.

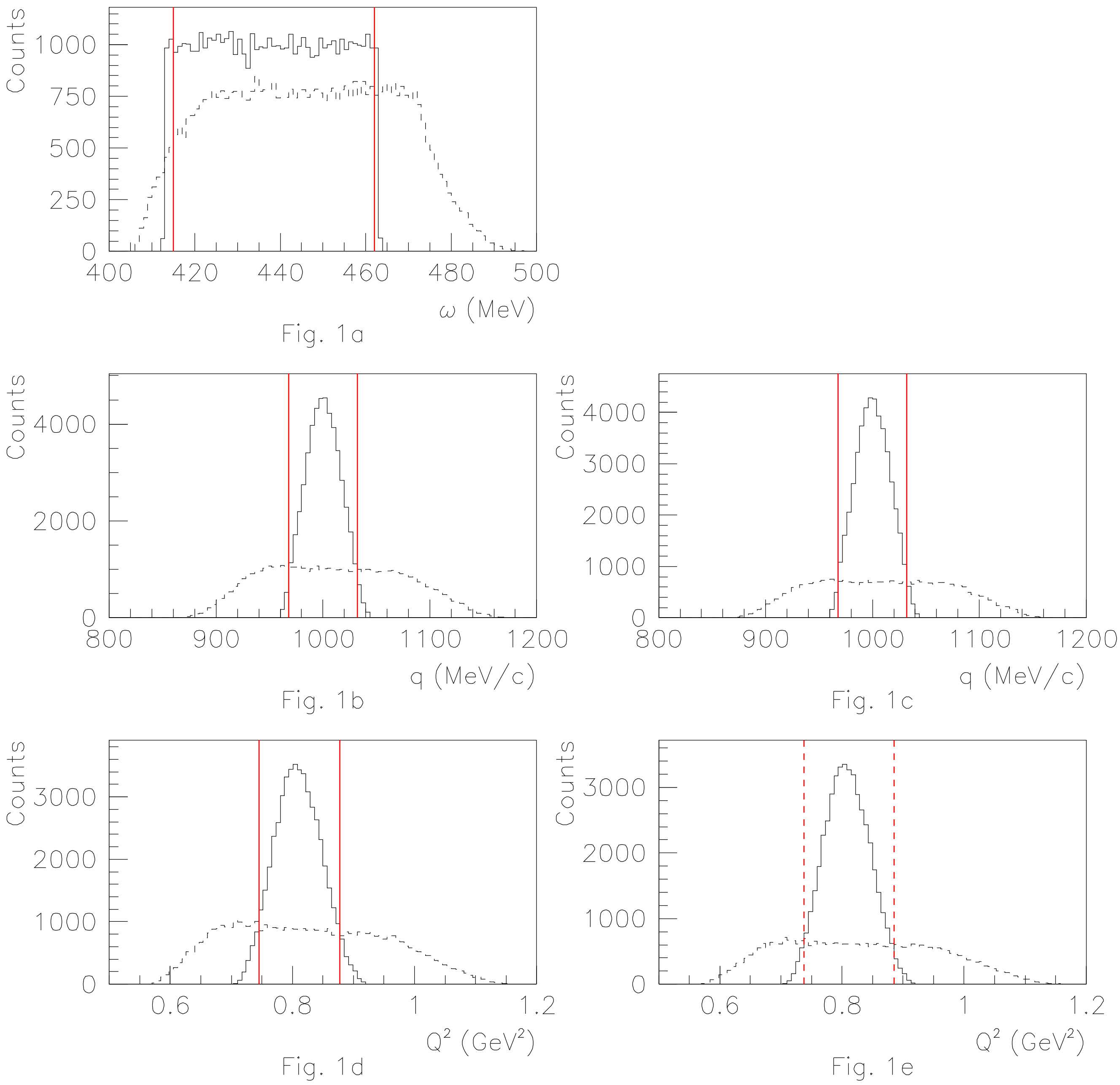

Figure 1.

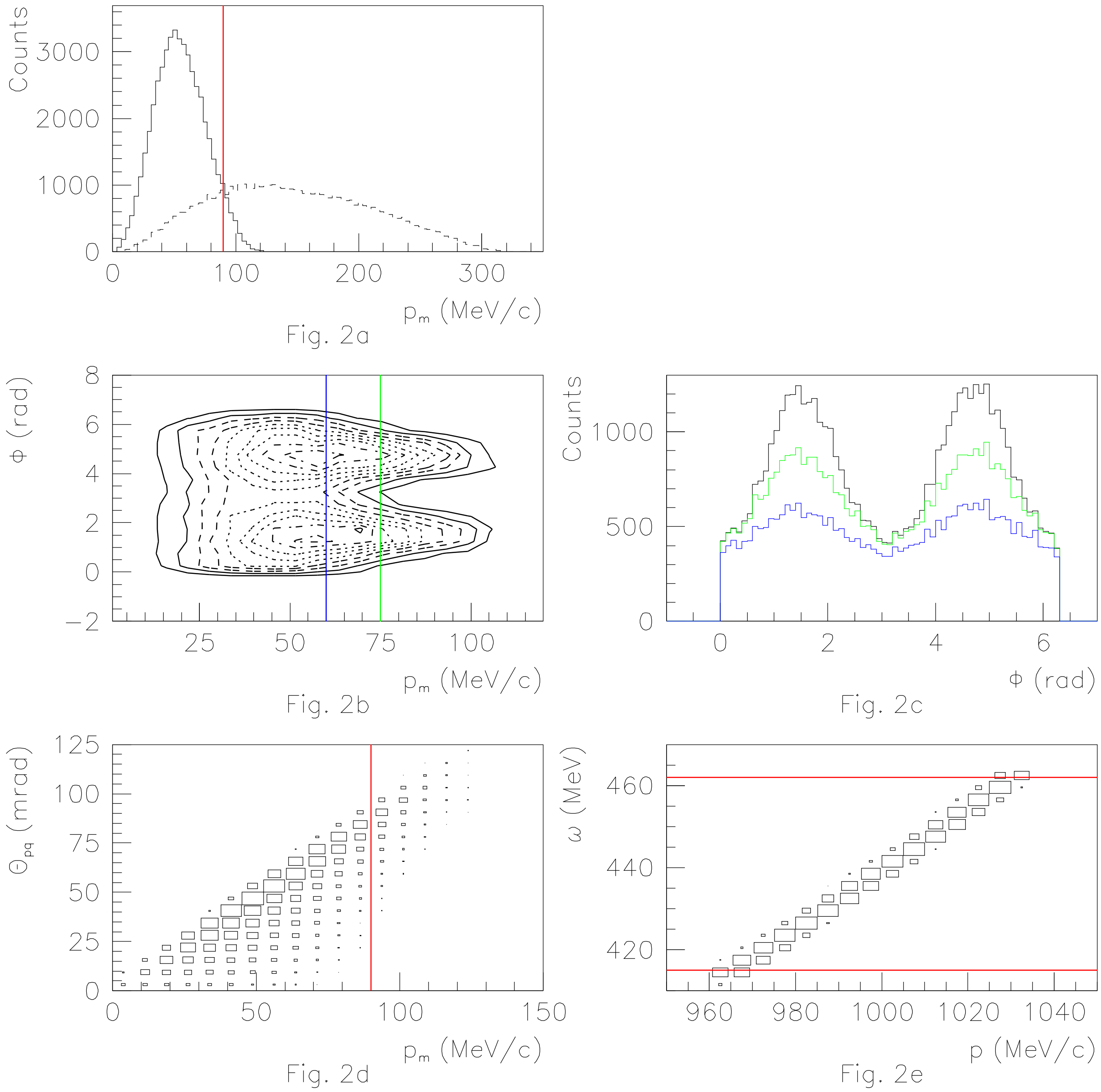
Counts
p_m (MeV/c)
Fig. 2a
φ (rad)
p_m (MeV/c)
Fig. 2b
Counts
φ (rad)
Fig. 2c
Θ_pq (mrad)
p_m (MeV/c)
Fig. 2d
ω (MeV)
p (MeV/c)
Fig. 2e

Figure 2.

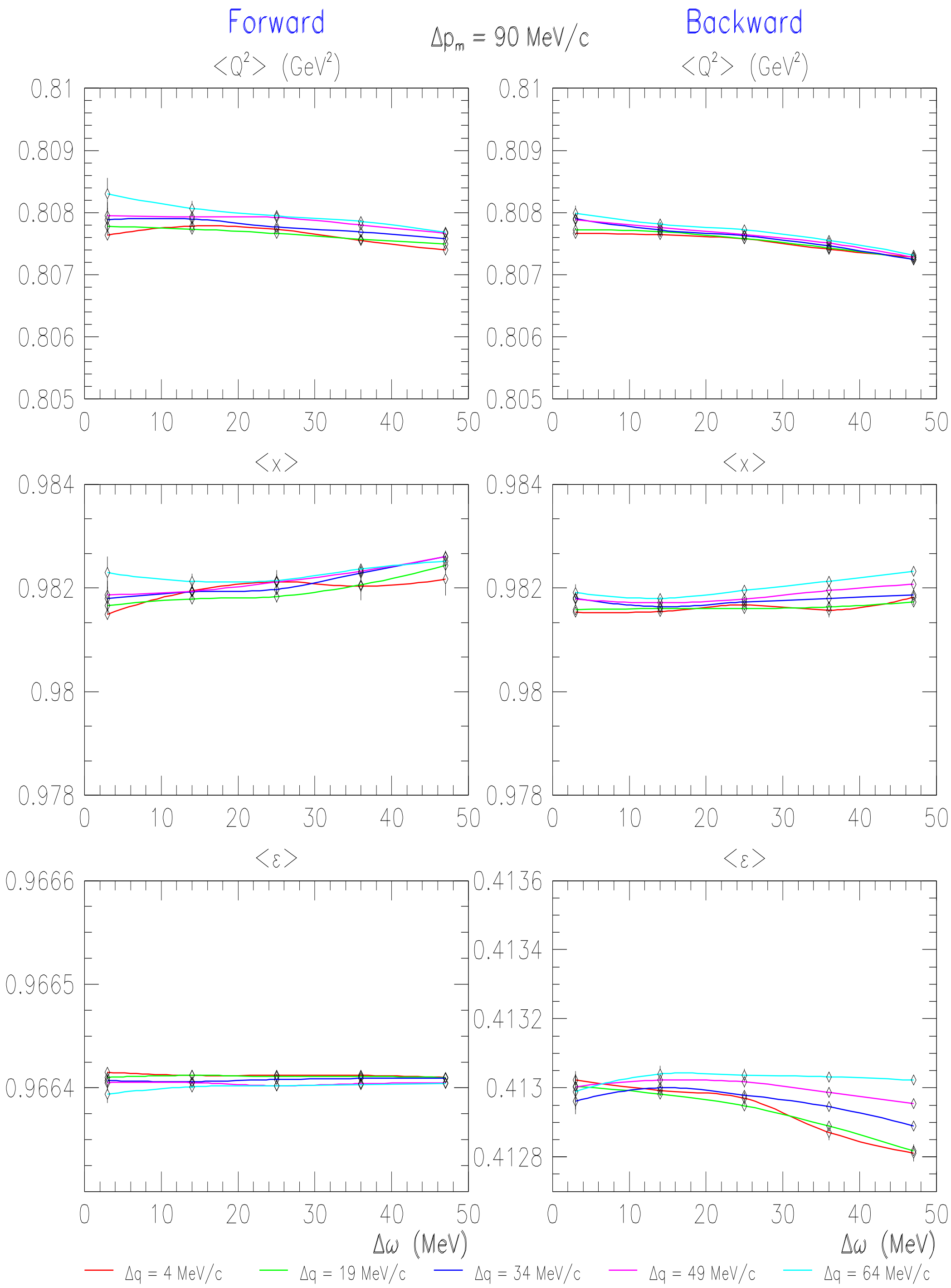

Forward
Backward
Δp_m = 90 MeV/c
<Q²> (GeV²)
<x>
<ε>
Δω (MeV)
Δq = 4 MeV/c
Δq = 19 MeV/c
Δq = 34 MeV/c
Δq = 49 MeV/c
Δq = 64 MeV/c

Figure 3.

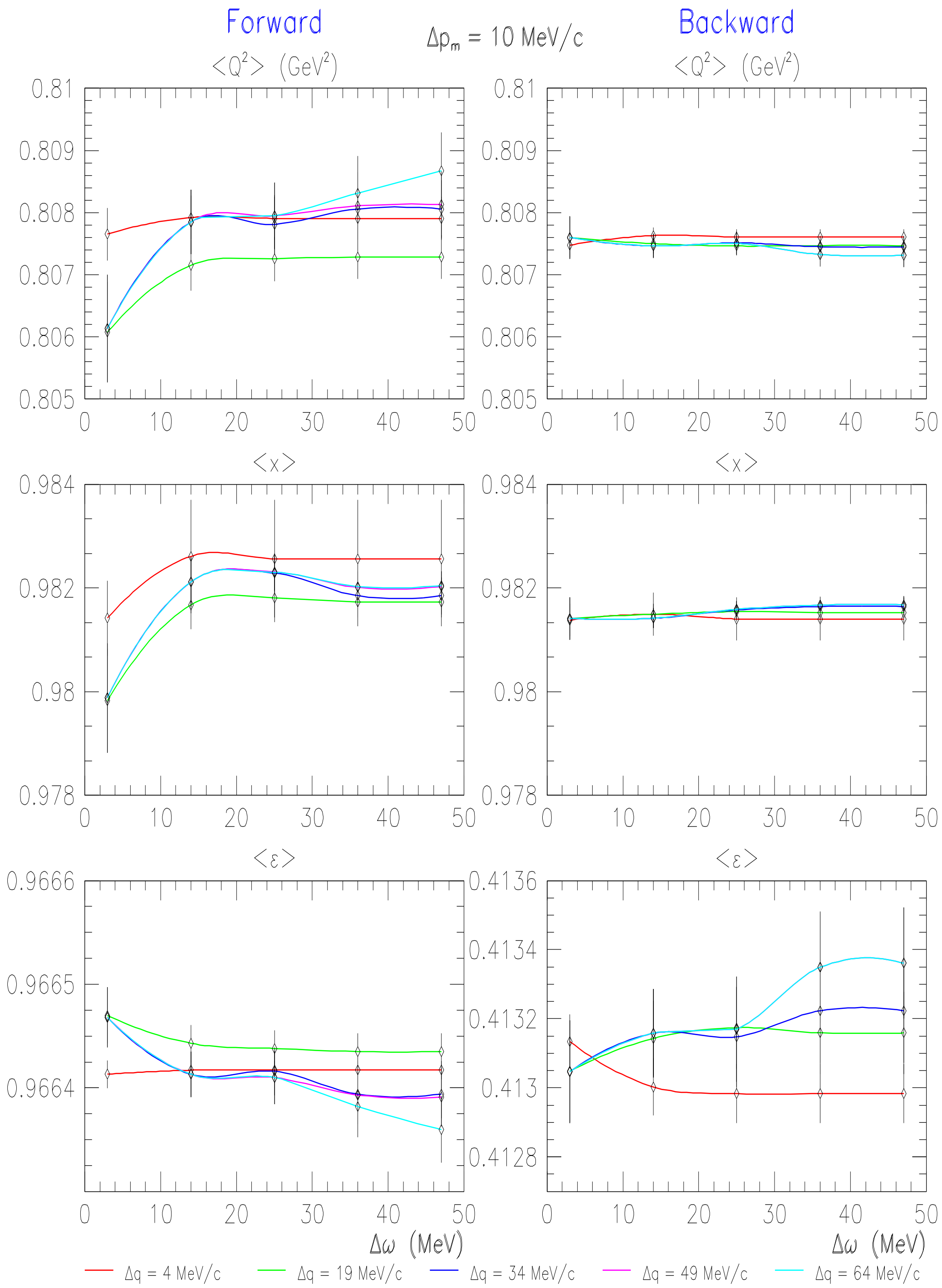
Forward
Δp_m = 10 MeV/c
Backward
$\langle Q^2 \rangle$ (GeV^2)
$\langle x \rangle$
$\langle \varepsilon \rangle$
$\Delta\omega$ (MeV)
Δq = 4 MeV/c
Δq = 19 MeV/c
Δq = 34 MeV/c
Δq = 49 MeV/c
Δq = 64 MeV/c

Figure 4.

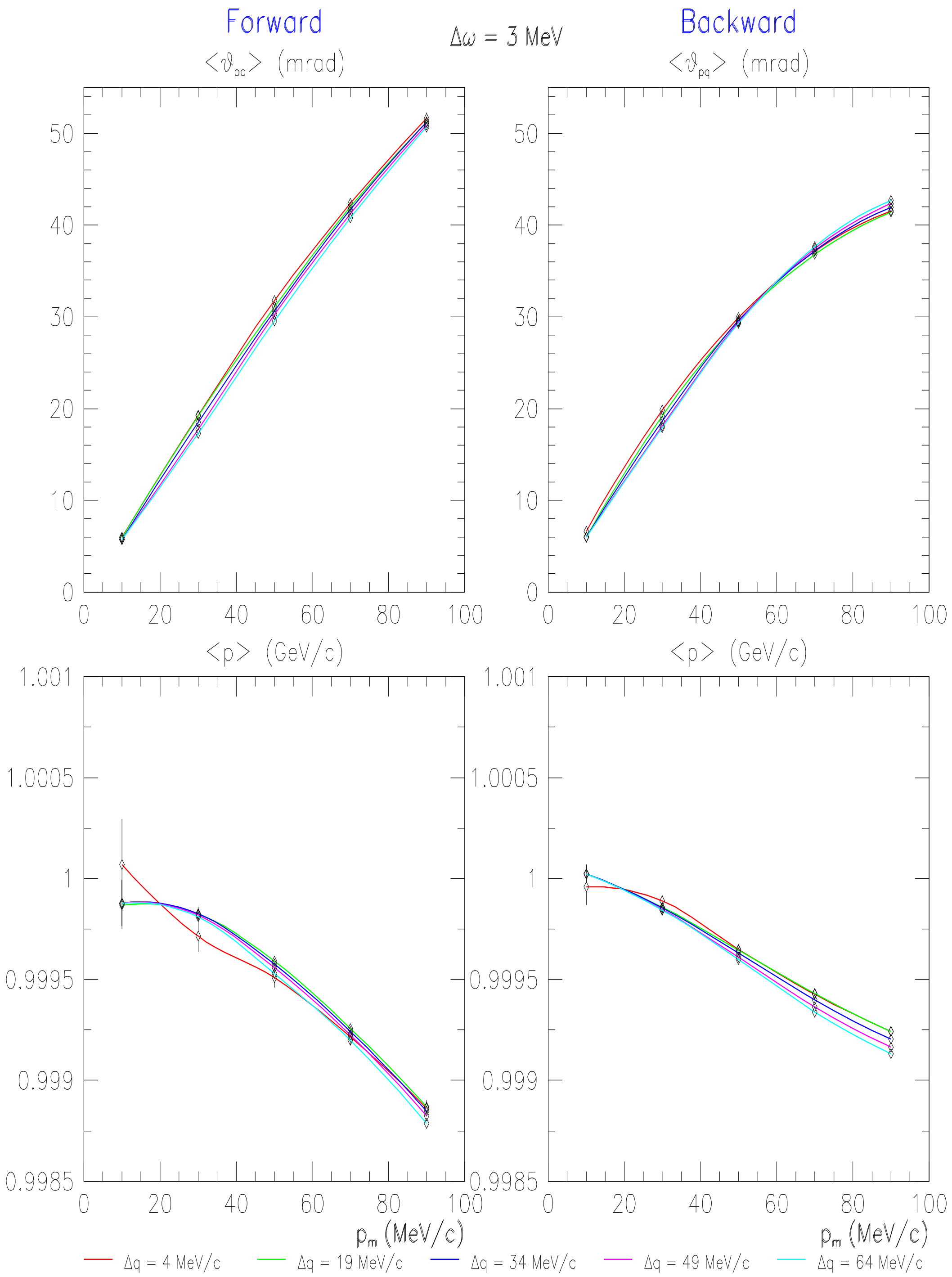
Forward
Δω = 3 MeV
Backward
<ϑ_pq> (mrad)
<ϑ_pq> (mrad)
<p> (GeV/c)
<p> (GeV/c)
p_m (MeV/c)
p_m (MeV/c)
Δq = 4 MeV/c
Δq = 19 MeV/c
Δq = 34 MeV/c
Δq = 49 MeV/c
Δq = 64 MeV/c

Figure 5.

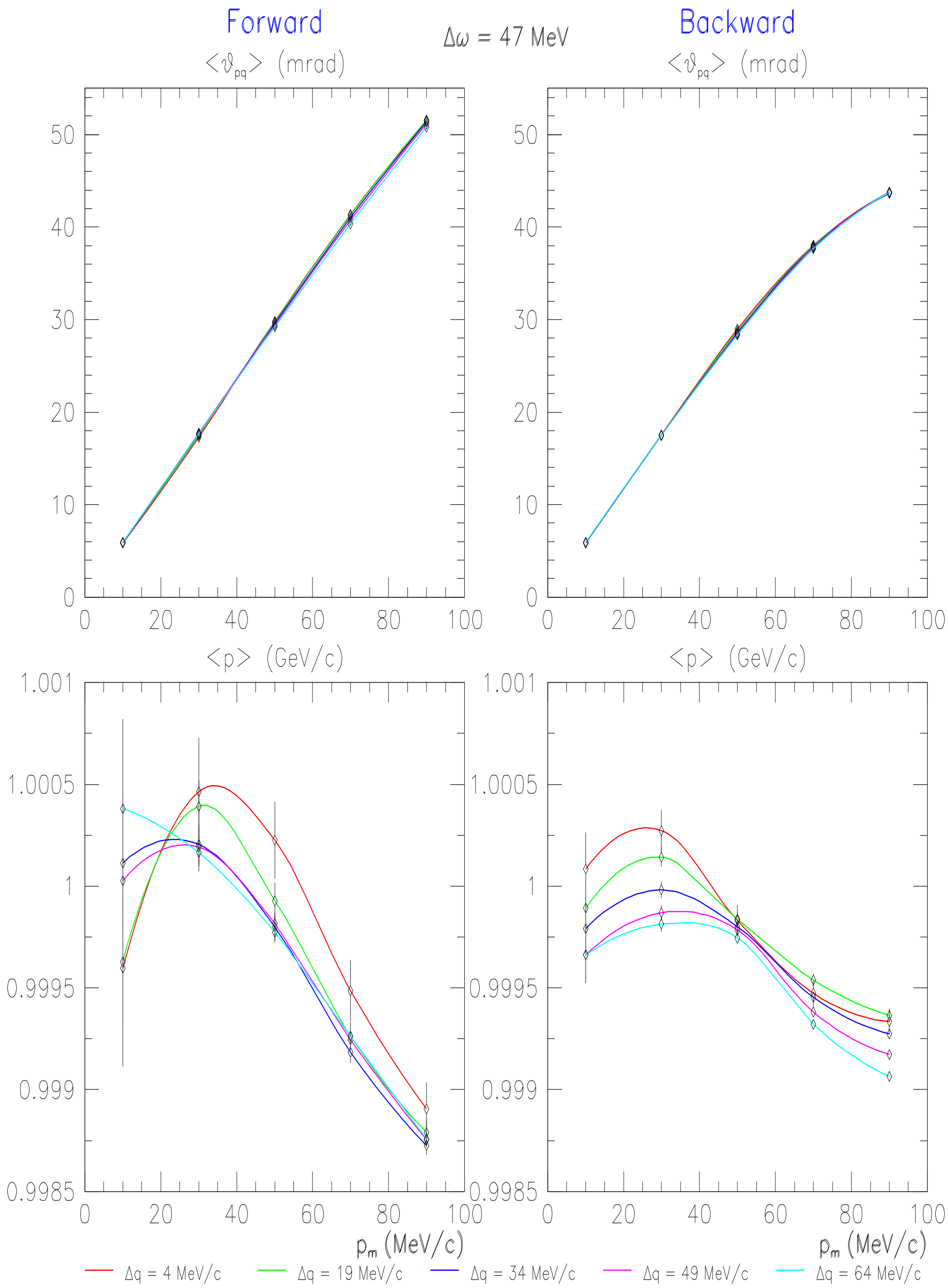
Forward
Δω = 47 MeV
Backward
<ϑpq> (mrad)
<ϑpq> (mrad)
<p> (GeV/c)
<p> (GeV/c)
pm (MeV/c)
pm (MeV/c)
Δq = 4 MeV/c
Δq = 19 MeV/c
Δq = 34 MeV/c
Δq = 49 MeV/c
Δq = 64 MeV/c

Figure 6.

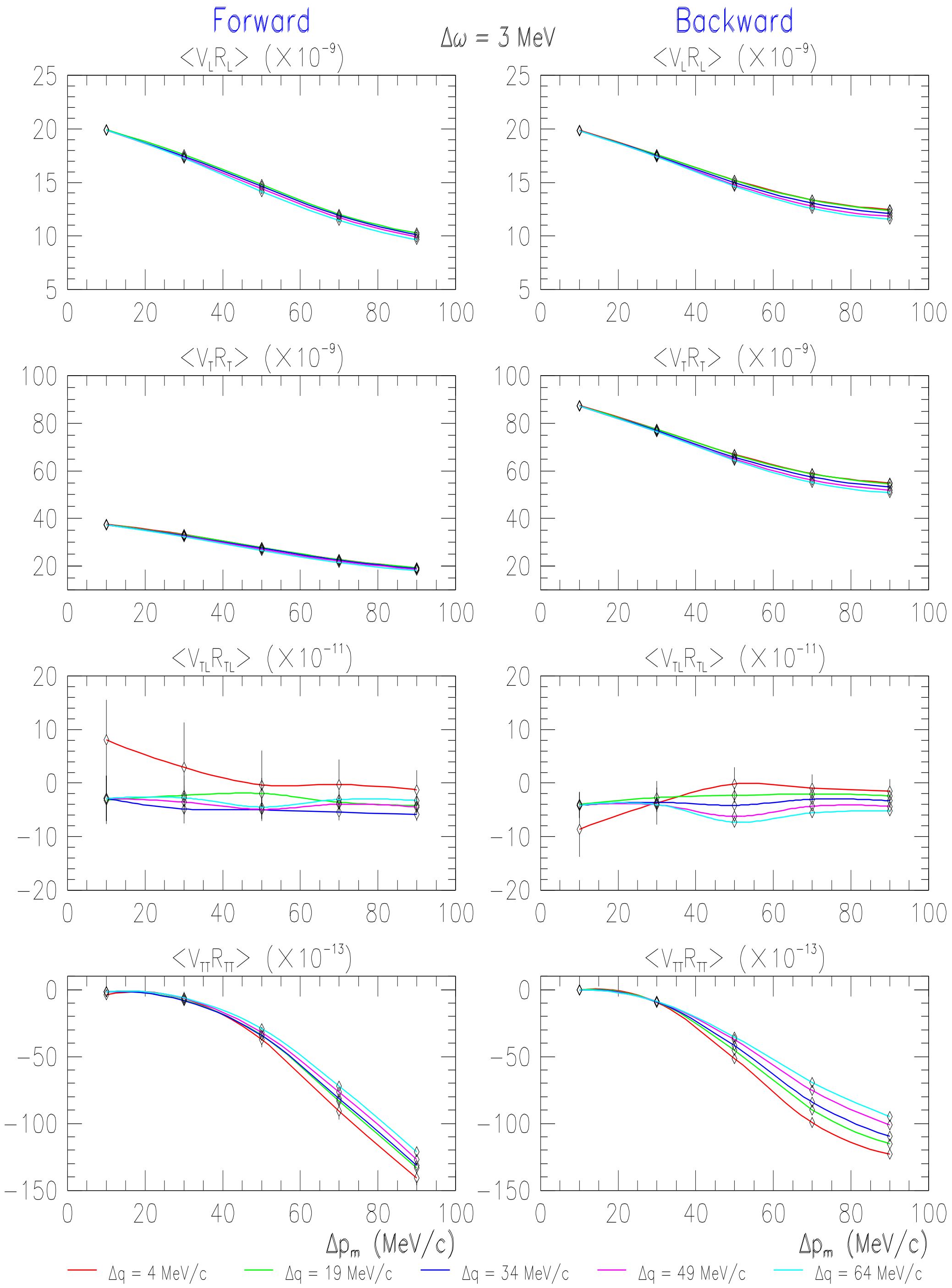

Forward
$\Delta\omega$ = 3 MeV
Backward
$\langle V_L R_L \rangle$ ($\times 10^{-9}$)
$\langle V_T R_T \rangle$ ($\times 10^{-9}$)
$\langle V_{TL} R_{TL} \rangle$ ($\times 10^{-11}$)
$\langle V_{TT} R_{TT} \rangle$ ($\times 10^{-13}$)
Δp_m (MeV/c)
Δq = 4 MeV/c
Δq = 19 MeV/c
Δq = 34 MeV/c
Δq = 49 MeV/c
Δq = 64 MeV/c

Figure 7.

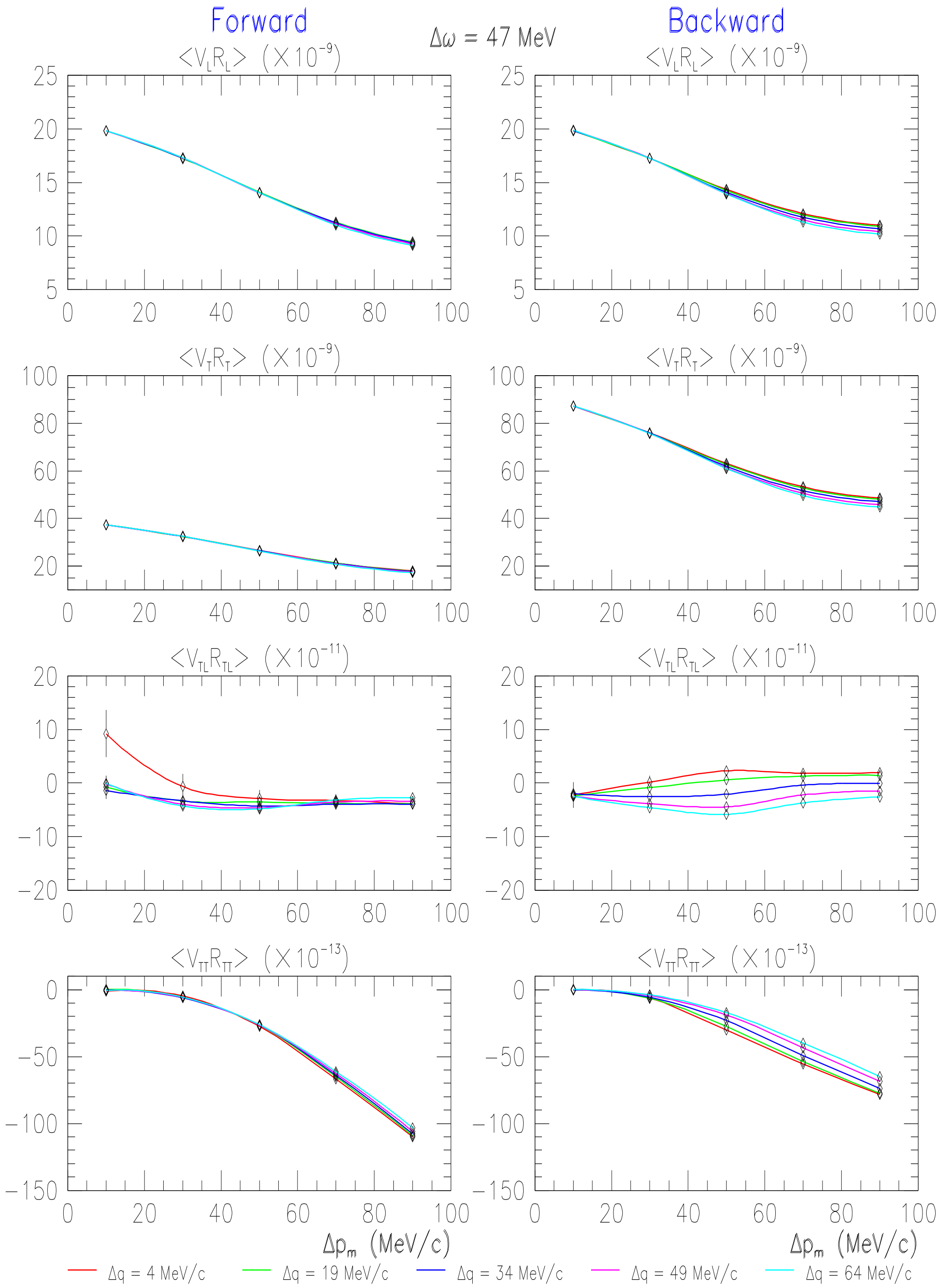
Forward
Backward
Δω = 47 MeV
<V_LR_L> (X10^-9)
<V_TR_T> (X10^-9)
<V_TLR_TL> (X10^-11)
<V_TTR_TT> (X10^-13)
Δp_m (MeV/c)
Δq = 4 MeV/c
Δq = 19 MeV/c
Δq = 34 MeV/c
Δq = 49 MeV/c
Δq = 64 MeV/c

Figure 8.

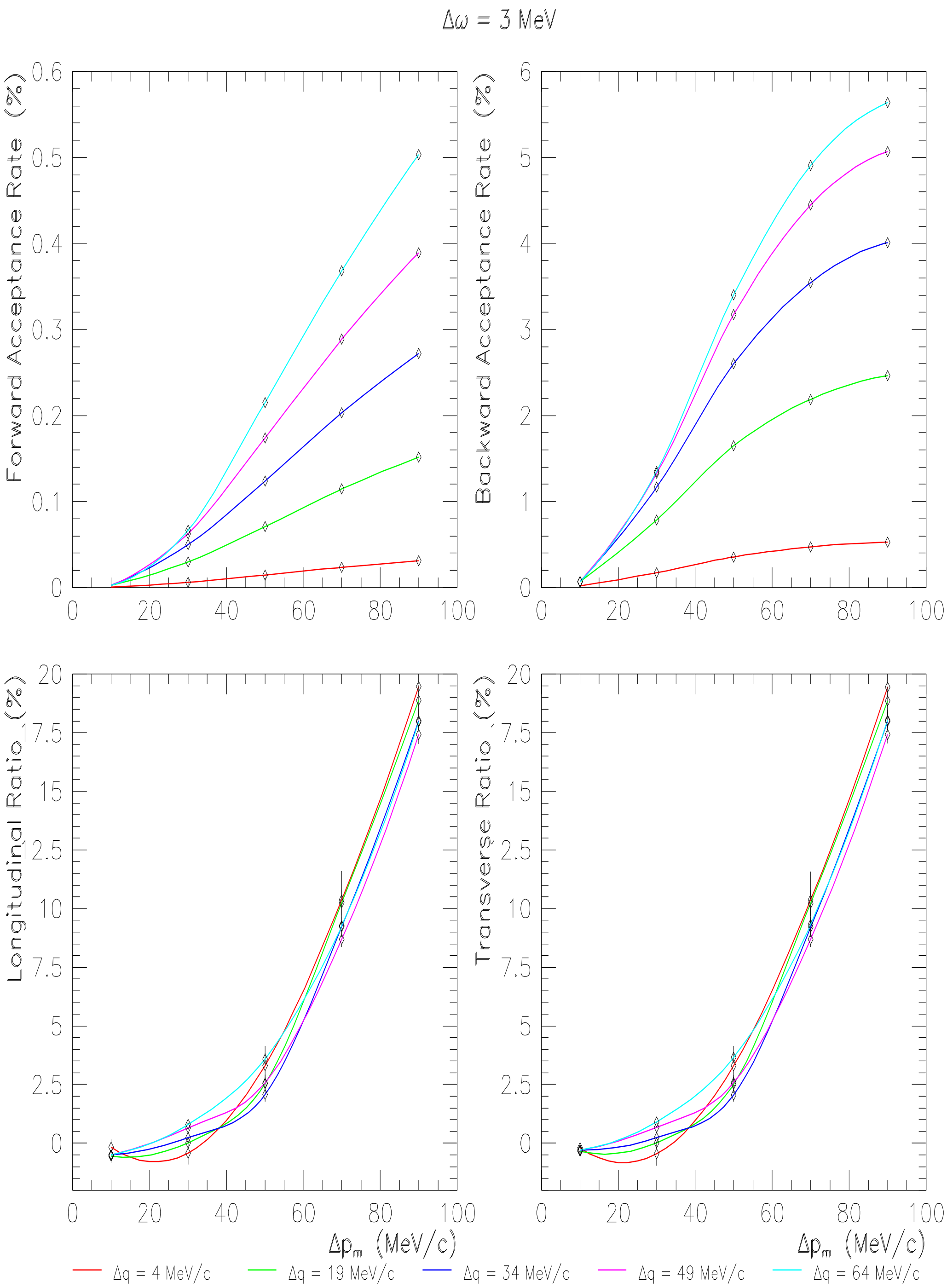
Δω = 3 MeV
Forward Acceptance Rate (%)
Backward Acceptance Rate (%)
Longitudinal Ratio (%)
Transverse Ratio (%)
Δp_m (MeV/c)
Δp_m (MeV/c)
Δq = 4 MeV/c
Δq = 19 MeV/c
Δq = 34 MeV/c
Δq = 49 MeV/c
Δq = 64 MeV/c

Figure 9.

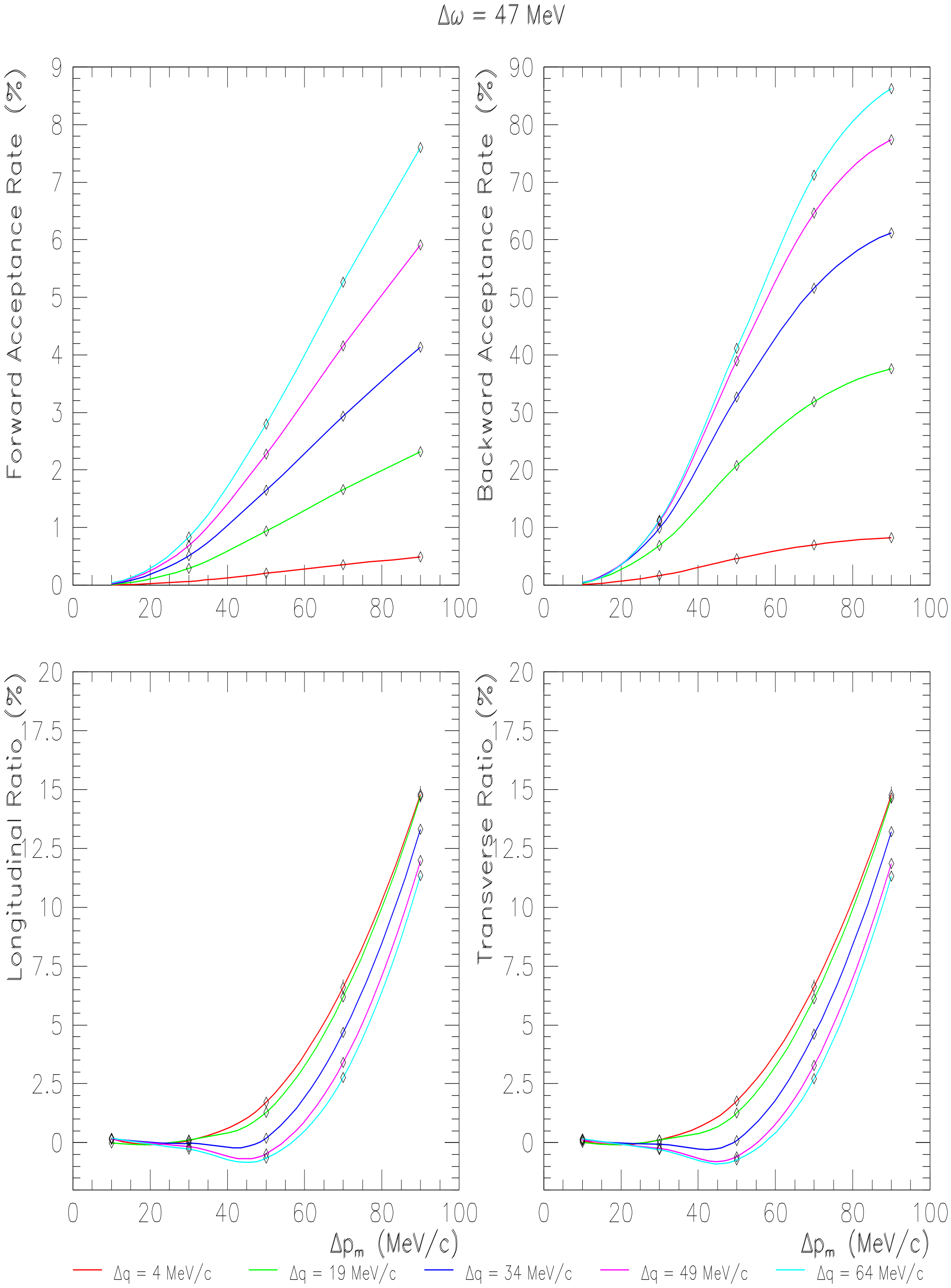

Δω = 47 MeV
Forward Acceptance Rate (%)
Backward Acceptance Rate (%)
Longitudinal Ratio (%)
Transverse Ratio (%)
Δp_m (MeV/c)
Δq = 4 MeV/c
Δq = 19 MeV/c
Δq = 34 MeV/c
Δq = 49 MeV/c
Δq = 64 MeV/c

Figure 10.